How many electron traps are formed in persistent phosphors?

AUTHOR(S):

Ueda, Jumpei; Xu, Jian; Takemura, Shota; Nakanishi, Takayuki; Miyano, Shun; Segawa, Hiroyo; Tanabe, Setsuhisa

CITATION:

Ueda, Jumpei ...[et al]. How many electron traps are formed in persistent phosphors?. ECS Journal of Solid State Science and Technology 2021, 10(11): 116003.

ISSUE DATE:

2021-10

ECS Journal of Solid State Science and Technology

The Electrochemical Society
Advancing solid state & electrochemical science & technology

OPEN ACCESS

How Many Electron Traps are formed in Persistent Phosphors?

To cite this article: Jumpei Ueda *et al* 2021 *ECS J. Solid State Sci. Technol.* **10** 116003

ECS Journal of Solid State Science and Technology, 2021 **10** 116003

How Many Electron Traps are formed in Persistent Phosphors?

Jumpei Ueda,[1,z] Jian Xu,[2] Shota Takemura,[3] Takayuki Nakanishi,[3] Shun Miyano,[1] Hiroyo Segawa,[3] and Setsuhisa Tanabe[1]

[1]*Graduate School of Human and Environmental Studies, Kyoto University, Yoshida-Nihonmatsu-cho, Sakyo-ku, Kyoto 606-8501, Japan*
[2]*International Center for Young Scientists (ICYS), National Institute for Materials Science (NIMS), Tsukuba, 305-0044, Japan*
[3]*National Institute for Materials Science (NIMS), Tsukuba, 305-0044, Japan*

Persistent luminescence is caused by a charge carrier detrapping process from the carrier traps filled by excitation light. Thus, the carrier storage capacity is an important factor in determining the persistent luminescence intensity. Here, the electron storage capacity was investigated in the YAGG:Ce^{3+}-Yb^{3+} transparent ceramic persistent phosphor, in which the Ce^{3+} ion is the luminescence center and the Yb^{3+} ion acts as the electron trap. The number density of the Yb^{2+} electron trapping center was estimated to be approximately 1.6×10^{18} ions cm^{-3} from the absorption coefficient spectrum of Yb^{2+}:4f–5d photochromic absorption center and the Yb-L_{III} edge XANES spectrum, which means that approximately 12% of the Yb^{3+} ions in the sample were changed to the divalent state after charging. Although the maximum energy density of 0.61 J cm^{-3} was calculated as a storage property of persistent phosphors from the Yb^{2+} number density and the photon energy of Ce^{3+}:$5d_1$−4f luminescence at 520 nm, the actual energy density which was detected as persistent luminescence was 0.011 J cm^{-3}. It is suggested that the recombination efficiency of the detrapped electrons from the Yb^{2+} ions with the hole-trapped Ce^{3+} ions is approximately a few percent.
 [DOI: 10.1149/2162-8777/ac2e4e]

Manuscript submitted September 1, 2021; revised manuscript received October 3, 2021. Published November 5, 2021. *This paper is part of the JSS Focus Issue on Focus Issue Dedicated to the Memory of George Blasse: Recent Developments in Theory, Materials, and Applications of Luminescence.*

Supplementary material for this article is available online

In 1967, Blasse and Bril reported an exceptional yellow phosphor of $Y_3Al_5O_{12}$:Ce^{3+} (Yttrium Aluminum Garnet doped with Ce^{3+}, YAG:Ce^{3+}),[1,2] which shows very broad 5d–4f luminescence band peaking at 550 nm,[1,2] high quantum efficiency (>95%),[3] short lifetime (∼60 ns)[4] and high quenching temperature (>800 K).[4–6] The YAG:Ce^{3+} phosphor that was developed more than 50 years ago is still one of the best yellow phosphors due to almost the perfect optical performance. It is widely known that a conventional white LED is composed of a blue LED and the YAG:Ce^{3+} phosphor. Blasse and Bril also reported that $Y_3Ga_5O_{12}$:Ce^{3+} (YGG:Ce^{3+}) does not show any luminescence by UV and blue light excitation, but the quenching process had not been elucidated for a long time.[2] In 2011, we investigated the quenching process using the photoconductivity technique and demonstrated that the quenching of YGG:Ce^{3+}: 5d–4f luminescence is caused by the photoionization process and that of $Y_3Al_2Ga_3O_{12}$:Ce^{3+} (YAGG:Ce^{3+}) is by the thermally-assisted photoionization process.[7]

Since the 4f electron of Ce^{3+} in the YAGG host is photoionized by blue light excitation, the YAGG:Ce^{3+}-based phosphors can become blue light chargeable persistent phosphors by introducing an appropriate electron trap such as Cr^{3+},[8,9] Sc^{3+}[10] or Yb^{3+} ions.[11] The developed YAGG:Ce^{3+}-based persistent phosphors show quite excellent persistent luminescence properties, for instance, the persistent luminescence duration of the Yb^{3+}-codoped one is 5600 min upon 0.32 mcd m^{-2}. On the other hand, the efficiency of persistent luminescence (storage capacity of electron traps) have not been investigated well quantitatively. It is very important and essential to know how many electrons can be trapped in the persistent phosphors in order to bring out the potential as a persistent phosphor. Van der Heggen et al. reported that only a fraction of Eu ions (approximately 1.6%) participated in the energy storage process and the maximum storage capacity is $(1.57 \pm 0.03) \times 10^{17}$ photons per gram for the $SrAl_2O_4$:Eu^{2+}-Dy^{3+} phosphor on the basis of absolute persistent luminescence decay analysis for transparent polymer samples containing the persistent phoshors.[12] Also, their estimation of the storage capacity was supported by the result of the change of Eu-L_{III} edge XANES peaks.[13]

In this study, the storage capacity by electron traps per volume was investigated in the YAGG:Ce^{3+}-Yb^{3+} transparent ceramics. The persistent luminescence of Ce^{3+} and the photochromic absorption of the Yb^{2+} ions can be evaluated per unit volume because the transparent bulk sample can be uniformly charged. In addition, the electron traps of the Yb^{2+} ions can be detected directly by the optical absorption and the Yb-L_{III} edge XANES spectra. From both measurement methods, the electron trap density was estimated to be approximately 1.6×10^{18} electrons cm^{-3}. We also discuss the persistent luminescence intensities with several units and the relationship between the persistent luminescence decay curve and the time-derivative absorption coefficient of Yb^{2+}: 4f–5d absorption band for the persistent luminescence mechanism.

Experimental

Transparent ceramics of $Y_3Al_2Ga_3O_{12}$ doped with 0.5% Ce^{3+} and 0.1% Yb^{3+} were prepared by solid-state reactions.[11] The specular transmittance spectra of as-made transparent ceramics were measured by a UV–VIS–NIR spectrometer (UV-3600, SHIMADZU). The time course of specular transmittance spectra during the charging process and detrapping process was also measured by the UV–vis-NIR spectrometer. For the charging process, the sample was illuminated by a 455 nm LED (LLS-455, OceanOptica) for different times (1, 3, 5, 10, 30 and 60 min). For the detrapping process, the spectrum was measured at several timings for 4 d after ceasing blue light charging. For persistent luminescence (PersL) spectra, the sample was charged by 450 nm monochromatic light by using a Xe lamp and a 450 nm bandpass filter and the persistent luminescence was detected by a CCD spectrometer (QE65PRO, Ocean Optics). After the sample was charged by the 450 nm monochromatic light mentioned above, the PersL decay curve was detected by a photomultiplier tube, PMT (R3896, Hamamatsu Photonics), which was covered with a 475 nm short-

[z]E-mail: ueda.jumpei.5r@kyoto-u.ac.jp

cut filter and a 600 nm long-cut filter to filter out all but the Ce^{3+} luminescence. The persistent radiance (mW Sr^{-1} m^{-2}) was measured by using a radiance-measurement setup (BW-L1, Konica-Minolta) composed of a CCD spectrometer (Glasier X, B&W Tek Inc.), a fiber and a collimator lens.

The X-ray absorption spectroscopy (XAS) was performed at the beamline BL-9A of Photon Factory (KEK, Japan). The Yb LIII X-ray absorption near edge structure (XANES) were recorded for the transparent ceramic sample charged by 450 nm laser (CPS450, Thorlabs) in the fluorescent mode using a solid state detector. The measured XANES spectra were treated by the pre-edge subtraction and the post-edge normalization using ATHENA software package.[14]

Molecular orbital (MO) calculation for a $[Yb(II)O_8]$ dodecahedron was performed by using the relativistic DV-Xα program.[15,16] For the accurate energy levels of Yb^{2+} was calculated by the relativistic discrete variational multi-electron (DVME) method developed by Ogasawara[17,18] using $[Yb(II)O_8]^{14-}$ cluster with lattice relaxation correction based on Shannon's crystal radii.[19]

Results and Discussion

Assignments of photo-induced absorption bands.—Figure 1a shows the absorption coefficient (α) spectra of the YAGG:Ce^{3+}(0.5)-Yb^{3+}(0.1%) transparent ceramics before and after charging by 455 nm light for 30 min. Before charging, Yb^{3+}: 4f–4f absorption lines from 900 nm to 1000 nm and Ce^{3+}: 4f–$5d_1$ and 4f–$5d_2$ absorption bands at 425 nm and 340 nm are observed. After charging, some additional absorption bands appear in the range from 250 nm to 800 nm. In order to clarify the photo-induced absorption centers, the difference spectrum, which is obtained by the subtraction of the absorption spectrum before charging from that after charging, is shown in Fig. 1b. A characteristic absorption band at 585 nm and some absorption bands below 400 nm are found to be generated. In the previous report, we assigned the absorption band at 585 nm to Yb^{2+}: 4f–5d on the basis of analogy with the reported Yb^{2+}: 4f–5d absorption band in $Y_3Al_5O_{12}$(YAG) and $Y_3Ga_5O_{12}$ (YGG).[11] However, it was also reported that the assignment of the broad absorption band from 500 nm to 700 nm in Yb^{2+}-doped $Y_3Al_5O_{12}$ is caused by the intervalence charge transfer (IVCT) between Yb^{2+} and Yb^{3+}.[20] In order to check the validity of Yb^{2+}: 4f–5d absorption from 500 nm to 700 nm, the 5d energy levels of YAG:Yb^{2+} were estimated by the ab-initio calculations. Figure 2a shows the energy levels of $Y_3Al_5O_{12}$:Yb^{2+} obtained by the DV-Xα molecular-orbital calculation method. Although the absolute energies of the calculated 5d levels have some energetic error, it is reasonable that the degenerated 5d energy level of Yb^{2+} is split to five different levels in $Y_3Al_5O_{12}$ like the case of Ce^{3+} in garnet crystals because the Y dodecahedral site with D_2 symmetry is distorted from the cubic symmetry (O_h).[21] In addition, there is a contribution of the Yb^{2+}: 6 s orbital, which results in the six split levels as excited states as shown in Fig. 2a. The observed lowest and second-lowest excited levels at 2.25 and 2.55 eV can be assigned to the lowest $5d_1$ and the second lowest $5d_2$ of Yb^{2+}, but the third to sixth levels at 3.80 eV to 4.40 eV in Fig. 2a are greatly mixed with the 5d and 6 s orbitals of Yb^{2+}.

In order to obtain more accurate 4f-5d absorption energies of the Yb^{2+} ions, the relativistic discrete variational multi-electron (DVME) method was used for the simulation of the absorption spectrum as shown in Fig. 2b. In the simulated absorption spectrum, the absorption band of Yb^{2+}-doped YAG with the lowest energy is located at 755 nm (1.64 eV), which is similar to the reported absorption band peak at 660 nm (1.88 eV).[20,22] Thus, the absorption bands at 660 nm in YAG:Yb^{2+} is not assigned to the IVCT band, but to the Yb^{2+}:4f–5d band. According to the calculation results, this absorption band at 660 nm is found to be formed mainly by the set of $5d_1$ and $5d_2$ (e_g level) of Yb^{2+}. The absorption below 400 nm in Fig. 2b can be attributed to the transition from Yb^{2+}: 4f to the

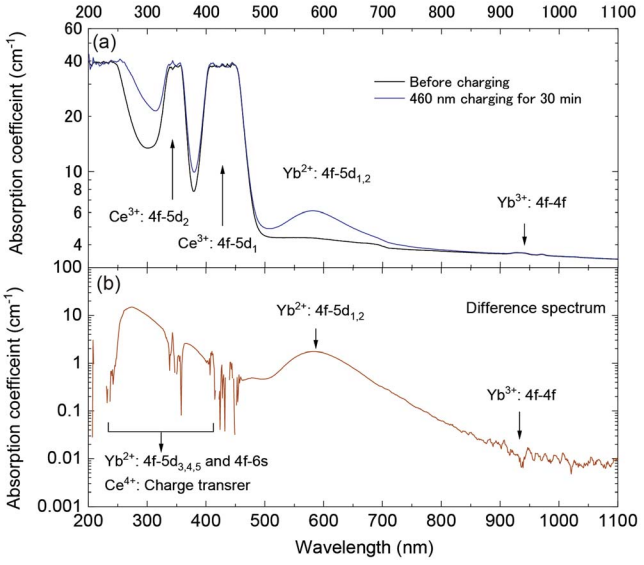

Figure 1. (a) Absorption coefficient spectra of YAGG:Ce^{3+}-Yb^{3+} transparent ceramics before charging (black solid line) and after charging by 455 nm blue LED for 30 min (blue solid line). Ce^{3+}:4f-$5d_1$ and $5d_2$ absorptions are saturated. (b) Difference spectrum of YAGG:Ce^{3+}-Yb^{3+} between the absorption spectra before and after charging.

excited state mixed with higher 5d energy levels (t_{2g} level) and 6 s level. The simulated absorption spectrum of YAG:Yb^{2+} is very similar to the difference spectrum of YAGG:Ce^{3+}-Yb^{3+} in Fig. 1b although the energy shifting is observed. Thus, the photo-induced absorption band at 585 nm can be assigned to the 4f–$5d_{1,2}$ absorption of Yb^{2+} and the absorption bands below 400 nm are related to Yb^{2+}:4f–$5d_{3,4,5}$ and 4f–6s. Also, the absorption band due to the LMCT (ligand to metal charge transfer) from O^{2-} to Ce^{4+} can participate in the difference spectrum in the UV region (below approximately 300 nm in YAG:Ce^{4+},[23–25]) since a part of the Ce^{3+} ions is photo-oxidized to the Ce^{4+} ions after blue light charging.

Estimation of Yb^{2+} fraction by XANES spectroscopy.—In order to check the existence of Yb^{2+} in the YAGG sample, the XANES spectrum for the Yb–L_{III} edge was measured. It is known that a charging process is caused by X-ray irradiation during the measurement of X-ray absorption spectrum.[13,26,27] Since the Yb valence state before the blue light charging process is difficult to be evaluated using the XANES spectrum due to the contribution of X-ray charging (see supporting information Fig. S1 available online at stacks.iop.org/JSS/10/116003/mmedia), the XANES spectrum of the sample fully charged by the 450 nm blue laser was analyzed as shown in Fig. 3. Two XANES bands are observed at 8940 eV and 8946 eV in the charged YAGG:Ce^{3+}-Yb^{3+} transparent ceramics. From the reference XANES spectra of Yb_2O_3 and CaF_2:$Yb^{3+/2+}$, the peaks at 8940 eV and 8946 eV are mainly contributed by the X-ray absorption of Yb^{2+} and Yb^{3+}, respectively (The XANES spectrum of CaF_2:Yb^{3+}/Yb^{2+} was traced from the Ref. 28). These results show that the charged YAGG:Ce^{3+}-Yb^{3+} transparent ceramic includes both Yb^{2+} and Yb^{3+}. In order to evaluate the ratio of Yb^{3+} and Yb^{2+} ions, the obtained XANES spectrum for the YAGG:Ce^{3+}-Yb^{3+} transparent ceramics is deconvoluted by two Gaussian functions for the main two absorption bands and an arctangent function for the continuous absorption. The obtained area can be evaluated directly as a ratio of Yb^{2+} and Yb^{3+} amount.[29] Based on the obtained area, it is found that the ratio of $Yb^{3+}$to Yb^{2+} is 82.5% to 17.5% in the charged YAGG:Ce^{3+}-Yb^{3+} persistent phosphor. Before charging, there is only an ignorable Yb^{2+}:4f–5d absorption in the optical absorption spectrum in the visible range (Fig. 1a). The observed Yb^{2+} center based on the XANES spectrum

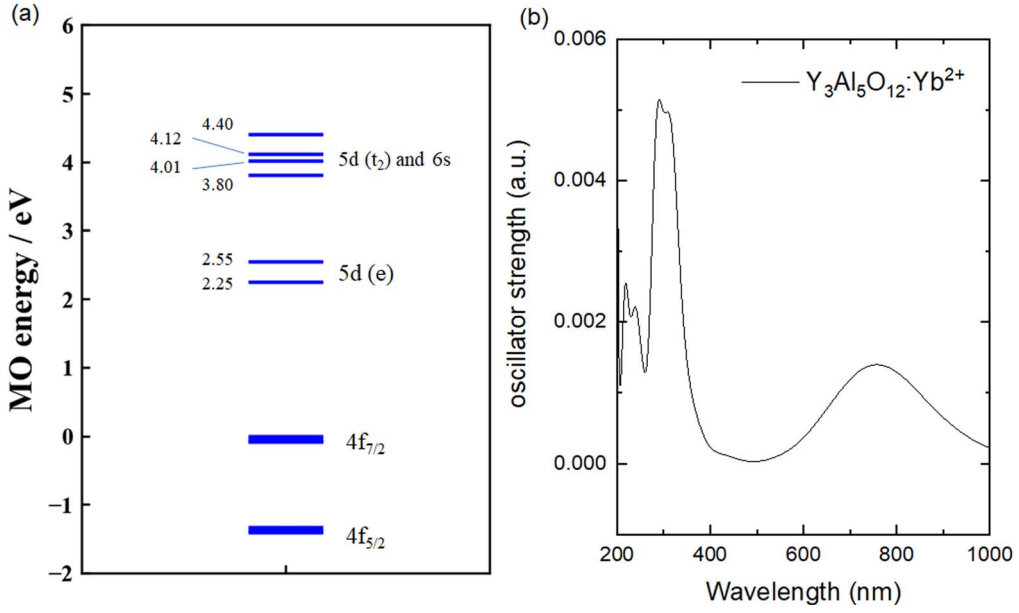

Figure 2. (a) Energy of the molecular orbital in [Yb(II)O_8] dodecahedron of $Y_3Al_5O_{12}$. (b) Simulated absorption oscillator strength of Yb^{2+}-doped $Y_3Al_5O_{12}$ based on the relativistic DVME method.

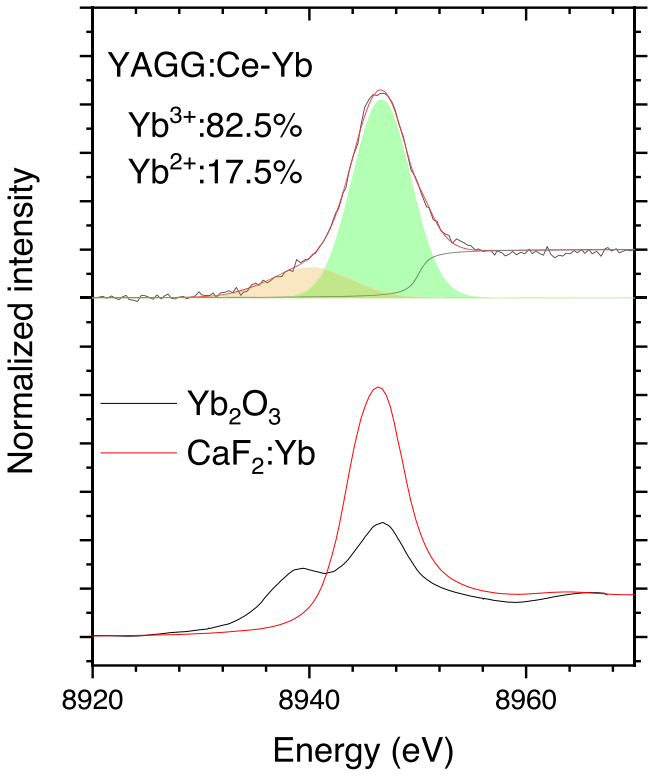

Figure 3. XANES spectra of Yb-L_{III} edge in $Y_3Al_2Ga_3O_{12}$:Ce^{3+}-Yb^{3+} after 450 nm blue laser charging with the reference spectra of Yb_2O_3 and CaF_2:Yb. The XANES spectrum of CaF_2:Yb^{3+}/Yb^{2+} was traced from the Ref. 28.

can be concluded to be formed by the charging process. The number density of Yb^{3+} in the sample before the charging process is 1.34×10^{19} ions cm^{-3} because the unit cell volume of $Y_3Al_2Ga_3O_{12}$ is 1795.91Å^3,[30] the 24 dodecahedral Y sites exist in the garnet unit cell, the Yb^{3+} concentration for Y site is 0.1% as the starting composition and the Yb^{3+} ions were not lost during synthesis. Thus, the photo-reduced Yb^{3+} (i.e. Yb^{2+}) after charging is determined to be approximately 2.35×10^{18} ions cm^{-3}.

Estimation of Yb^{2+} number density by optical absorption spectroscopy.—Figures 4a and 4b shows the time dependence of the Yb^{2+} absorption coefficient spectra in the YAGG:Ce^{3+}-Yb^{3+} transparent ceramics for the charging process and for the detrapping process. The Yb^{2+}:4f–5d absorption increases with increasing charging time and is almost saturated at 60 min charging. After stopping blue LED charging, the Yb^{2+}:4f–5d absorption intensity decreases with time gradually. These results also show that the Yb^{2+} ion is the electron trapping center. From the obtained absorption coefficient spectra, we also estimated the number density of the Yb^{2+} ions. The oscillator strength of the absorption band in the range between 500 nm to 900 nm in Yb^{2+}-doped YAG was reported to be 5.25×10^{-3} [20]. The oscillator strength can be expressed by

$$f = 4\pi\varepsilon_0 \frac{9m_e c^2 n}{Ne^2\pi(n^2+2)^2}\int \alpha d\sigma, \qquad [1]$$

where f is the oscillator strength, m_e is the electron mass, c is the speed of light, ε_0 is the vacuum dielectric constant, n is the refractive index, N is the number density of ions, e is the elementary electronic charge, α is the absorption coefficient, and σ is wavenumber.[31–33] Assuming the oscillator strength of Yb^{2+}:4f–5d in YAGG is the same as that in YAG, the Yb^{2+} number density in the charged YAGG:Ce^{3+}-Yb^{3+} sample can be estimated by obtaining the integrated absorption coefficient and the refractive index. The integrated absorption coefficient of Yb^{2+}:4f–$5d_{1,2}$ absorption for the sample charged for 60 min by the blue LED in the range between 500 nm to 900 nm is estimated to 6956 cm^{-2}. Because the refractive index of $Y_3Al_2Ga_3O_{12}$ has not been reported, the refractive index (1.9353) of YGG:Nd^{3+} was used.[34] As a result, the number density of Yb^{2+} is estimated to be 8.58×10^{17} ions cm^{-3}, which is slightly smaller than the estimation by the XANES absorption.

Estimation of total photon number for persistent luminescence.—We already reported the persistent luminescence decay curve with luminance (mcd m^{-2}) of the YAGG:Ce^{3+}-Yb^{3+} transparent ceramics.[11] The luminance is a good parameter for the non-transparent persistent phosphor samples while for the transparent samples, such as transparent ceramics and single crystal, the luminance increases with increasing thickness of the sample.[35,36] This feature is an advantage to obtain higher persistent luminescence intensity, whereas it is a problem for the comparison of the persistent

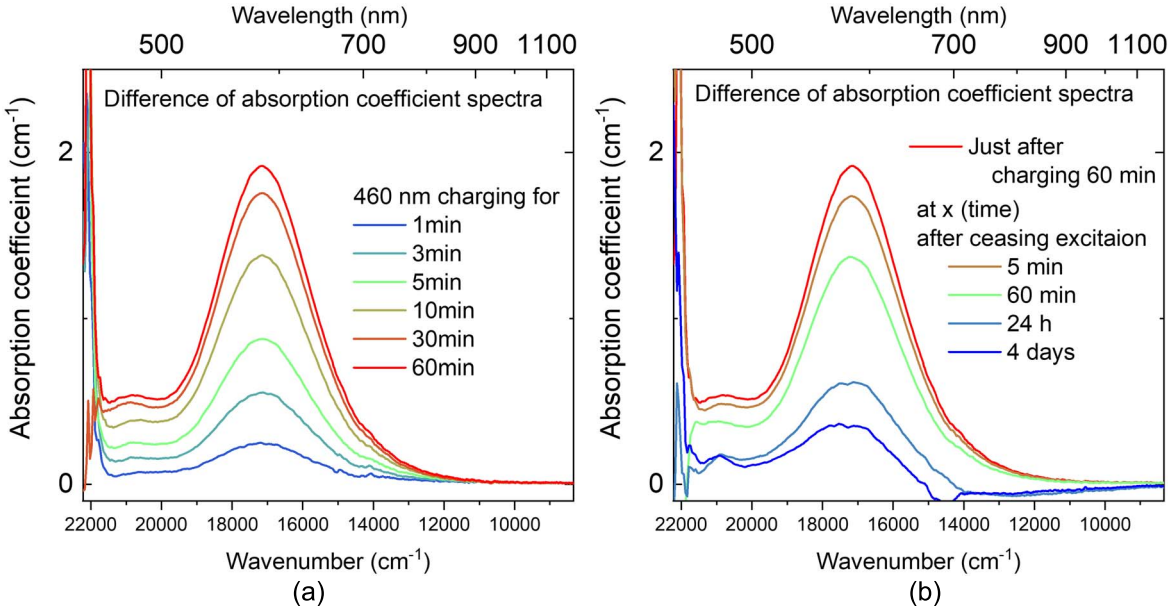

Figure 4. Time dependence of difference spectra (a) charging process and (b) detrapping process.

luminescence intensity among the samples. Thus, for the transparent persistent phosphors, the persistent luminescence intensity per volume should be discussed. In addition, the luminance (mcd m^{-2}) depends significantly on the luminescence wavelength, so that the unit should be related to the photon number[37] for the discussion of physics behind the persistent luminescence phenomenon. Originally, we obtained the persistent luminescence spectrum in the radiance unit (mW sr^{-1} m^{-2}) by the radiance meter and converted to luminance by taking into account the spectral luminous efficiency curve (lm W^{-1}). Also, the persistent luminescence spectra with radiance unit can be converted to the phonon radiance (cps sr^{-1} m^{-2}) by dividing by the photon energy. Here, the thickness of the YAGG:Ce^{3+}-Yb^{3+} transparent ceramics tereated in this research is 2.1 mm. Thus, the photon intensity density (cps sr^{-1} cm^{-3}) can be calculated by dividing the photon radiance by the thickness. Moreover, the total photon flux density (cps cm^{-3}) can be estimated by multiplying the photon intensity density by the total solid angle of 4π. As a result, the persistent luminescence decay curve with the total photon flux density can be obtained as shown in Fig. 5. By integrating the persistent decay curve in time, the total photon number density can be estimated. However, the persistent luminescence decay curve was measured only until 1200 min, which will underestimate the integration area. Thus, the persistent luminescence decay curve in the log-log plot was fitted by a quadratic function and extrapolated to enough long time to obtain the total photon number density. As a result, that value was estimated to be 2.88×10^{16} photons cm^{-3}.

Persistent luminescence induced by electron detrapping from Yb^{2+}.—From the absorption and XANES spectra, it is obvious that Yb^{3+} ions act as electron traps. However, a new question arises: Is the Ce^{3+} persistent luminescence caused really by the electron detrapping from Yb^{2+}? The persistent luminescence (I_{PersL}) is proportional to the detrapping rate of electron traps($-dn_e/dt$), which is also related to the time-derivative absorption coefficient of electron traps ($-d\alpha/dt$).[38]

$$I_{PersL} \propto -\frac{dn_e}{dt} \propto -\frac{d\alpha}{dt}. \qquad [2]$$

Therefore, we can discuss the persistent luminescence mechanism by the relationship between the persistent luminescence decay curve and the time-derivative absorption coefficient of the electron traps.

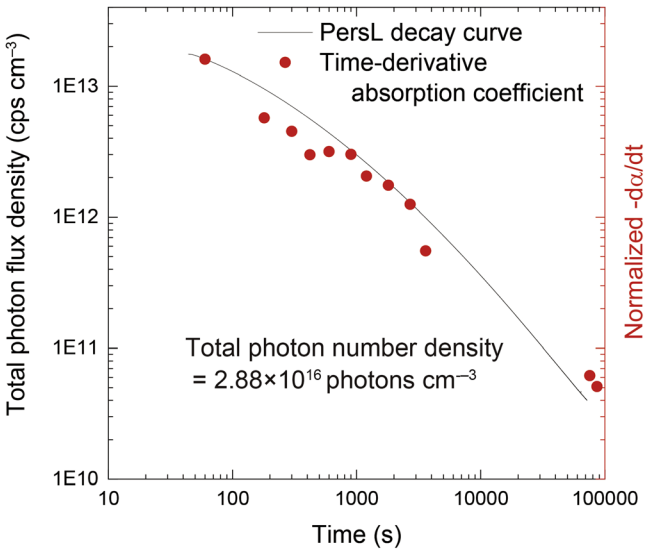

Figure 5. Persistent luminescence decay curve with total photon flux density (cps cm^{-3}) of YAGG:Ce^{3+}-Yb^{3+} transparent ceramics and the time-derivative absorption coefficient of Yb^{2+}:4f–$5d_{1,2}$ absorption band which is normalized at 1 min.

In Fig. 5, the normalized time-derivative absorption coefficient of Yb^{2+} absorption after stopping the charging process is also plotted. The decreasing tendency of the time derivative absorption coefficient of Yb^{2+}:4f–$5d_{1,2}$ shows good agreement with the Ce^{3+}:5d–4f persistent luminescence decay curve. This is strong evidence that the electrons detrapped from the Yb^{2+} traps cause the persistent luminescence of Ce^{3+} ions.

Comparison of electron trap density and persistent luminescence intensity.—Table I summarizes the number density of Yb^{2+} ions and the ratio of Yb^{2+}/Yb^{3+} estimated by three different analyses. For the PersL decay curve, the total photon number density was obtained as shown in Fig. 5. If we assume that the Ce^{3+} PersL was caused only by the detrapping process from Yb^{2+} and the recombination efficiency is unity, the Yb^{2+} number density and the ratio of Yb^{2+}/Yb^{3+} can be estimated. However, the Yb^{2+} number density is smaller than that estimated by the absorption and

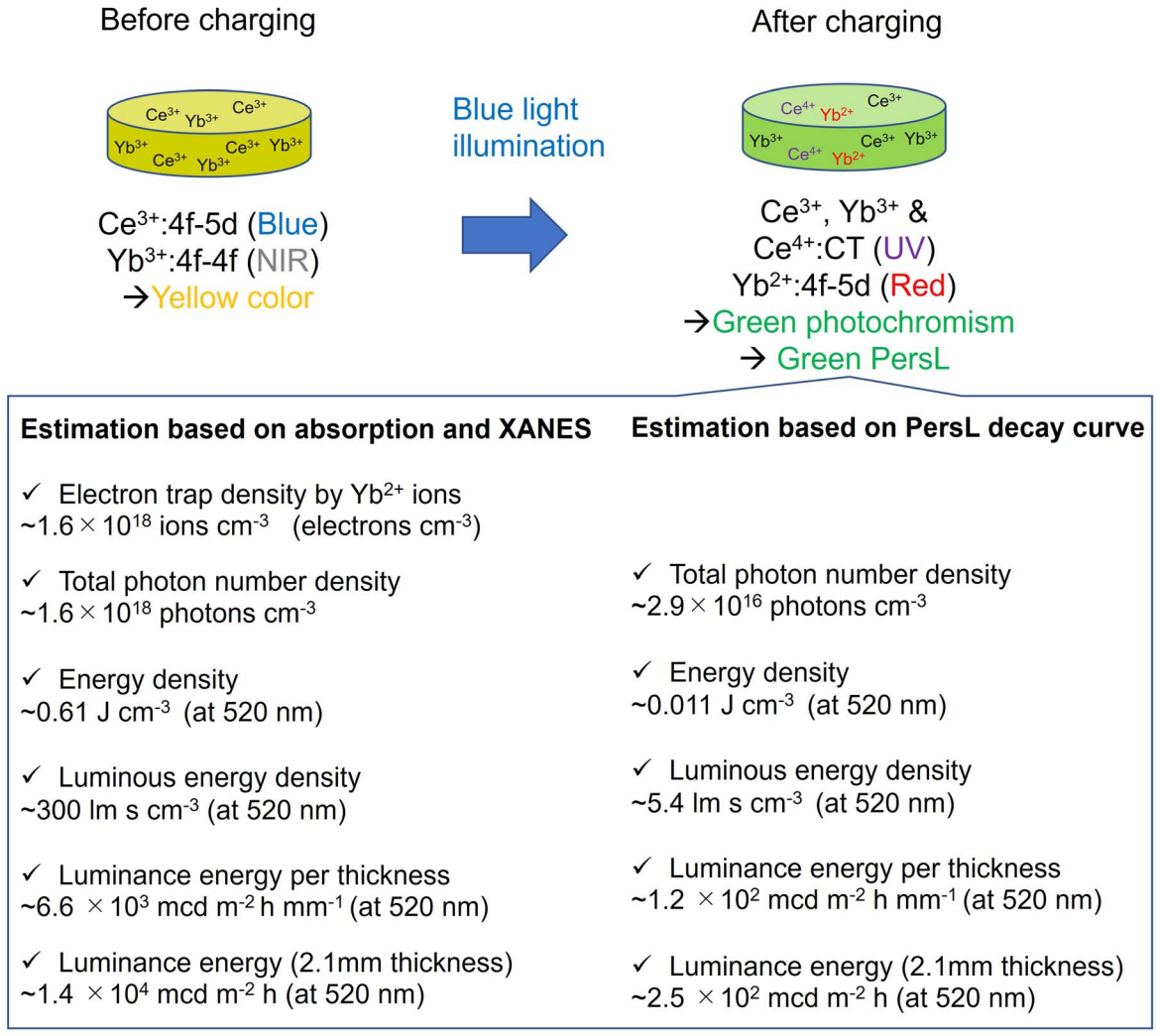

Figure 6. Schematic image of valence stage changing by charging process and the estimation of values related to storage capacity.

Table I. Comparison of number density and ratio of Yb^{2+}/Yb^{3+} estimated by three different analyses.

	Yb^{2+} absorption	Yb L_{III} XANES	PersL
Number densities of Yb^{2+} ions or photons	0.858×10^{18} ions cm^{-3}	2.35×10^{18} ions cm^{-3}	2.88×10^{16} photons cm^{-3}
Ratio of Yb^{2+}/Yb^{3+}	6.17%	17.5%	0.214%

the XANES spectroscopy by two orders of magnitudes as shown in Tabel I. This result shows the recombination efficiency is far from unity. Based on the number density of Yb^{2+} obtained in the absorption and XANES spectroscopy, the recombination efficiencies are estimated to be 3.5% and 1.2%, respectively. These recombination efficiencies are smaller compared with the quantum yield (QY 73.5%) of Ce^{3+}:$5d_1-4f$ luminescence in $Y_3Al_2Ga_3O_{12}$ by blue light excitation.[21] These results indicate that the most of detrapped electrons are directly recombined nonradiatively with the hole-trapped Ce^{3+} ions without going through the 5d excited state of Ce^{3+}.

The number densities of Yb^{2+} in the charged sample were estimated by the absorption spectroscopy and the XANES spectroscopy to be 0.858×10^{18} ions cm^{-3} and 2.35×10^{18} ions cm^{-3}, respectively. There are some differences depending on the analysis method, but those values are similar to each other in the order of magnitude. The difference may come from some reasons: One possibility is the overestimation of oscillator strength,[20] leading to the smaller number density of Yb^{2+} for the absorption coefficient analysis. As the other possibility, the different charging condition in the absorption and XANES spectroscopies causes the deviation of the number of electron traps despite of the condition with enough strong power and long time charging process to achieve the saturation of electron traps. The calculated ratios of Yb^{2+}/Yb^{3+} from the optical absorption and XANES measurements are 6.17% and 17.5%, respectively. Here, we assumed that averagely 12% of Yb^{3+} ions in the YAGG:Ce^{3+}(0.5%)-Yb^{3+}(0.1%) were changed into the divalent state by blue light charging process, which indicates that 2.4% of the Ce^{3+} ions changes into a tetravalent state and participate in the persistent luminescence process.

The 12% change from Yb^{3+} to Yb^{2+} by the charging process in the YAGG:Ce^{3+}(0.5%)-Yb^{3+}(0.1%) sample means that the approximately 1.6×10^{18} electrons are trapped per one cubic centimeter, which can generate the persistent luminescence with 1.6×10^{18} photons cm^{-3} at maximum (Fig. 6) Considering the photon energy (3.82×10^{-19} J) and the luminous efficacy (485 lm W^{-1}) at 520 nm, which is the peak wavelength of Ce^{3+}:$5d_1-4f$ luminescence, one can convert the photon number density to 0.61 J cm^{-3} (energy

density) and 300 lm s cm^{-3} (luminous energy density). These values are a kind of maximum energy density by assuming that all the trapped electrons can convert to persistent luminescence at 520 nm. For the persistent phosphors, the luminance (mcd m^{-2}) can be widely used for the comparison of persistent luminescence performance. If we can compare the general luminance to luminous energy density directly, it helps to understand the persistent luminescence intensity. Here, when the transparent ceramic persistent phosphor of YAGG:Ce^{3+}-Yb^{3+} with the 1 mm thickness is considered, the 300 lm s cm^{-3} luminous energy density can be converted to 6.6 × 10^3 mcd m^{-2} h mm^{-1} as the luminance energy per one-milimeter thickness, which means that this persistent phosphor with 1 mm thickness has the ability to emit the persistent luminescence with the continuous value of 6.6 × 10^3 mcd m^{-2} for 1 h or 6.6 × 10^2 mcd m^{-2} for 10 h and so on. This idea is similar to the discharge capacity with the mAh unit for the battery area.

On the other hand, we cannot withdraw all the charged energy in the YAGG:Ce^{3+}-Yb^{3+} as persistent luminescence due to the low recombination efficiency as discussed above. Based on the total photon numbers of Ce^{3+} persistent luminescence, the recombination efficiency was found to be ranged from 1.2% to 3.5% (the average is 2.4%). When we calculate the energy density, luminous energy density and luminance energy per one-milimeter thickness based on the obtained persistent luminescence decay curve with total photon flux density, the values are estimated to be ∼0.011 J cm^{-3}, 5.4 lm s cm^{-3} and 1.2 × 10^2 mcd m^{-2} h mm^{-1}, respectively. For instance, we can say that the YAGG:Ce^{3+}-Yb^{3+} transparent ceramic persistent phosphor with 1 mm thickness has the ability to show 120 mcd m^{-2} luminance for 1 h. We can also use the luminance energy (mcd m^{-2} h) for the persistent phosphors in which the sample thickness cannot be determined or for the persistent phosphors with specific thickness. For instance, the YAGG:Ce^{3+}-Yb^{3+} transparent ceramics with 2.1 mm thickness has 2.5 × 10^2 mcd m^{-2} h luminance energy based on the persistent luminescence decay curve. We cannot determine the real persistent duration from the luminance energy because the actual persistent luminescence intensity declines gradually with time. The luminance energy (per thickness) is one of the expression methods of the storage capacity for the persistent phosphors.

Conclusions

The photochromic absorption band at 585 nm after blue light charging in the $Y_3Al_2Ga_3O_{12}$:Ce^{3+}-Yb^{3+} transparent ceramic persistent phosphor was confirmed to be the 4f–5d absorption of Yb^{2+} electron trapping center based on the Molecular orbital (MO) calculation. The formation of Yb^{2+} ions were also demonstrated by the XANES spectroscopy. The Yb^{2+} number density were calculated to be 1.6 × 10^{18} ions cm^{-3} from the absorption coefficient spectrum of Yb^{2+}:4f–5d photochromic center and the Yb-L_{III} edge XANES spectrum. Based on the obtained number density of Yb^{2+}, it is found that approximately 12% of Yb^{3+} in the sample was changed into a divalent state by the charging process. Assuming that all of the Yb^{2+} electron trapping centers can generate the Ce^{3+} persistent luminescence at 520 nm, the YAGG:Ce^{3+}-Yb^{3+} transparent ceramic persistent phosphor is regarded to store the energy with the energy density of 0.61 J cm^{-3}. On the other hand, the measured energy density from the persistent luminescence decay curve with the total photon flux per volume is 0.011 J cm^{-3}. This result indicates that the recombination efficiency after the detrapping process is only a few percent. The storage capacity estimated from the Yb^{2+} number density and the persistent luminescence intensity was compared in several units such as energy density (J cm^{-3}), luminous energy density (lm s cm^{-3}) and luminance energy (per thickness). We suggested that the luminance energy per thickness (mcd m^{-2} h mm^{-1}) and luminance energy (mcd m^{-2} h) are one of the good expression methods of the storage capacity for the persistent phosphors. In addition, for the persistent luminescence mechanism, because the time-derivative absorption coefficient ($-d\alpha/dt$) of the Yb^{2+}:4f–5d absorption corresponds to the Ce^{3+} persistent luminescence decay curve, it was concluded that the Ce^{3+} persistent luminescence can be caused by the electron detrapping from the Yb^{2+} ions.

Acknowledgments

This work was financially supported by No., 20H02438, 18KK0405 and 19H02798 from the Japan Society for the Promotion of Science (JSPS). The XANES measurements have been performed under the approval of the Photon Factory Program Advisory Committee (No. 2020G105).

ORCID

Jumpei Ueda https://orcid.org/0000-0002-7013-9708
Jian Xu https://orcid.org/0000-0002-1040-5090
Shota Takemura https://orcid.org/0000-0003-3462-0032
Takayuki Nakanishi https://orcid.org/0000-0003-3412-2842
Hiroyo Segawa https://orcid.org/0000-0002-7198-8410
Setsuhisa Tanabe https://orcid.org/0000-0002-7620-0119

References

1. G. Blasse and A. Bril, *Appl. Phys. Lett.*, **11**, 53 (1967).
2. G. Blasse and A. Bril, *J. Chem. Phys.*, **47**, 5139 (1967).
3. S. Nishiura, S. Tanabe, K. Fujioka, and Y. Fujimoto, *IOP Conf. Ser.: Mater. Sci. Eng.*, **18**, 102005 (2011).
4. M. J. Weber, *Solid State Commun.*, **12**, 741 (1973).
5. V. Bachmann, C. Ronda, and A. Meijerink, *Chem. Mater.*, **21**, 2077 (2009).
6. J. Ueda, P. Dorenbos, A. J. J. Bos, A. Meijerink, and S. Tanabe, *The Journal of Physical Chemistry C*, **119**, 25003 (2015).
7. J. Ueda, S. Tanabe, and T. Nakanishi, *J. Appl. Phys.*, **110**, 053102 (2011).
8. J. Ueda, K. Kuroishi, and S. Tanabe, *Appl. Phys. Lett.*, **104**, 101904 (2014).
9. J. Ueda, P. Dorenbos, A. J. J. Bos, K. Kuroishi, and S. Tanabe, *J. Mater. Chem. C*, **3**, 5642 (2015).
10. J. Ueda, A. Hashimoto, S. Takemura, K. Ogasawara, P. Dorenbos, and S. Tanabe, *J. Lumin.*, **192**, 371 (2017).
11. J. Ueda, S. Miyano, and S. Tanabe, *ACS Appl. Mater. Interfaces*, **10**, 20652 (2018).
12. D. Van der Heggen, J. Joos, D. Rodríguez Burbano, J. Capobianco, and P. Smet, *Materials*, **10**, 867 (2017).
13. K. Korthout, K. Van den Eeckhout, J. Botterman, S. Nikitenko, D. Poelman, and P. F. Smet, *Physical Review B*, **84**, 085140 (2011).
14. B. Ravel and M. Newville, *J. Synchrotron Radiat.*, **12**, 537 (2005).
15. H. Adachi, M. Tsukada, and C. Satoko, *J. Phys. Soc. Jpn.*, **45**, 875 (1978).
16. A. Rosén, D. E. Ellis, H. Adachi, and F. W. Averill, *J. Chem. Phys.*, **65**, 3629 (1976).
17. K. Ogasawara, T. Ishii, I. Tanaka, and H. Adachi, *Physical Review B*, **61**, 143 (2000).
18. K. Ogasawara, T. Iwata, Y. Koyama, T. Ishii, I. Tanaka, and H. Adachi, *Physical Review B*, **64**, 115413 (2001).
19. S. Watanabe, T. Ishii, K. Fujimura, and K. Ogasawara, *J. Solid State Chem.*, **179**, 2438 (2006).
20. M. Kreye and K. D. Becker, *Phys. Chem. Chem. Phys.*, **5**, 2283 (2003).
21. J. Ueda and S. Tanabe, *Optical Materials: X*, **1**, 100018 (2019).
22. M. Henke, J. Perßon, and S. Kück, *J. Lumin.*, **87–89**, 1049 (2000).
23. A. Nagura, K. Kamada, M. Nikl, S. Kurosawa, J. Pejchal, Y. Yokota, Y. Ohashi, and A. Yoshikawa, *Jpn. J. Appl. Phys.*, **54**, 04DH17 (2015).
24. A. D. Sontakke, J. Ueda, J. Xu, K. Asami, M. Katayama, Y. Inada, and S. Tanabe, *The Journal of Physical Chemistry C*, **120**, 17683 (2016).
25. M. V. Derdzyan, K. L. Hovhannesyan, A. V. Yeganyan, R. V. Sargsyan, A. Novikov, A. G. Petrosyan, and C. Dujardin, *CrystEngComm*, **20**, 1520 (2018).
26. J. Ueda, M. Katayama, K. Asami, J. Xu, Y. Inada, and S. Tanabe, *Opt. Mater. Express*, **7**, 2471 (2017).
27. J. J. Joos, K. Korthout, L. Amidani, P. Glatzel, D. Poelman, and P. F. Smet, *Phys. Rev. Lett.*, **125**, 033001 (2020).
28. T. Yoshida, H. Kagi, H. Tsuno, A. Ohta, and M. Nomura, *Chem. Lett.*, **34**, 852 (2005).
29. T. Tanaka, T. Hanada, S. Yoshida, T. Baba, and Y. Ono, *Jpn. J. Appl. Phys.*, **32**, 481 (1993).
30. A. Nakatsuka, A. Yoshiasa, and T. Yamanaka, *Acta Crystallographica section B*, **55**, 266 (1999).
31. B. Henderson and G. F. Imbusch, *Optical Spectroscopy of Inorganic Solids* (Clarendon, Oxford) (2006).
32. Y. Sun, C. W. Thiel, and R. L. Cone, *Physical Review B*, **85**, 165106 (2012).
33. R. Fukumori, Y. Huang, J. Yang, H. Zhang, and T. Zhong, *Physical Review B*, **101**, 214202 (2020).
34. Y. Lili, L. Yong, L. Shuang, F. Gang, Y. Qingyang, and Z. Jinhua, *Opt. Mater. Express*, **9**, 1907 (2019).
35. J. Ueda, K. Kuroishi, and S. Tanabe, *Appl. Phys. Express*, **7**, 062201 (2014).
36. J. Xu, J. Ueda, K. Kuroishi, and S. Tanabe, *Scr. Mater.*, **102**, 47 (2015).
37. J. Xu and S. Tanabe, *J. Lumin.*, **205**, 581 (2019).
38. J. Ueda, A. Hashimoto, and S. Tanabe, *The Journal of Physical Chemistry C*, **123**, 29946 (2019).